International Journal of Heat and Mass Transfer 226 (2024) 125444

Contents lists available at ScienceDirect

International Journal of Heat and Mass Transfer

journal homepage: www.elsevier.com/locate/ijhmt

Modeling of a liquid nitrogen droplet evaporating inside an immiscible liquid pool

Z. Zhang [a,*], H. Zhao [b], S. Vanapalli [a,*]

[a] Applied Thermal Sciences Lab, University of Twente, Enschede, Post bus 217, 7500 AE, Overijssel, the Netherlands
[b] Wolfson School of Mechanical, Electrical and Manufacturing Engineering, Loughborough University, Loughborough, Leicestershire LE11 3TU, UK

ARTICLE INFO

Keywords:
Liquid nitrogen
Droplet evaporation
Leidenfrost phenomena
Bubble growth

ABSTRACT

Evaporation of liquid nitrogen in another immiscible liquid occurs in many industrial applications. Existing oversimplified one-dimensional (1D) quasi-steady models, although can quantitatively predict the evaporation rate by introducing an empirical fitting parameter, rely on configurations inconsistent with experimental observation so more rigorous models are required to get in-depth physical insights and improve modeling capability. This study proposes a 2D quasi-steady-state theoretical model, free of fitting parameters, that predicts the bubble growth rate and estimates the heat transfer rate for a liquid nitrogen droplet evaporating inside a liquid pool within the spherical bubble regime. The droplet's shape and position within a spherical bubble are determined by the equilibrium between the gravitational force and the upward pressure force resulting from the vapor flow between the droplet and the pool. The vapor layer thickness is calculated to be on the order of 10 microns. Notably, the primary contribution to heat transfer arises from the lower portion of the droplet, leading to local heat flux values up to approximately six times higher at the bottom compared to the top. The predicted bubble growth is quantitatively consistent with experimental data within the capillary spherical bubble regime. Furthermore, the overall heat transfer rate Q exhibits a distinct scaling relationship with the volume ratio between the bubble and droplet, yielding $Q \sim (V_b/V_d)^{-0.1}$.

1. Introduction

Reliable and accurate temperature control is indispensable for the food supply chain, which extends across various domains like food processing, product packaging, storage & transportation as well as retail service [1–3]. The latent heat associated with Liquid Nitrogen (LN_2) phase change enables an ultra-fast cooling of the entire volume of the product within just a few minutes of exposure to liquid nitrogen. This cooling power makes it possible to achieve fast, uniform, and efficient cooling, along with quality preservation using LN_2. In addition to food-freezing applications in which the internal temperature of food is brought down below the freezing point, LN_2 is also a preferred candidate for liquid chilling in which temperatures are maintained above the freezing point. This has applications in the beverage sector, for chilling packaged or bottled beverages. By injecting nitrogen directly into hot sauces, soups, dips, marinades, or fruit purees, the temperature of the products is reduced from around 90 °C to 4 °C in just a few seconds.

Fast evaporation of liquid nitrogen is also desirable in various industrial applications such as cooling concrete [4–6], cryogenic engines [7–9]. To achieve fast evaporation of liquid nitrogen, many existing studies proposed and studied the evaporation of a liquid nitrogen jet inside a hot fluid, in particular liquids that have a much higher heat capacity than the gas [10–13]. However, the limited heat transfer area raises doubts about the reliability of effective heat transfer rates. Therefore, instead of using a liquid cryogen jet, an atomized cryogenic spray can be employed to enhance the evaporation rate considerably by increasing the interfacial area [14]. A cryogenic spray usually consists of multiple droplets. It is necessary to be able to model the evaporation of a single LN_2 drop accurately before modeling the whole spray.

Liquid nitrogen droplets used for food and beverage chilling are typically very small, with diameters lying around 0.1 mm [15], which is much less than the capillary length l_{c_d}. This is primarily because the rapid cooling effect of liquid nitrogen is most effective when there is a larger surface-area-to-volume ratio resulting in more efficient heat transfer [14]. The capillary length l_{c_d} of a droplet is defined as $\sqrt{\sigma_d/(\rho_d g)}$, where ρ_d and σ_d are the density and surface tension of the droplet, respectively, and g is the gravitational acceleration. The capil-

* Corresponding authors.
E-mail addresses: z.zhang-3@utwente.nl (Z. Zhang), s.vanapalli@utwente.nl (S. Vanapalli).

https://doi.org/10.1016/j.ijheatmasstransfer.2024.125444
Received 4 October 2023; Received in revised form 9 February 2024; Accepted 12 March 2024
Available online 25 March 2024

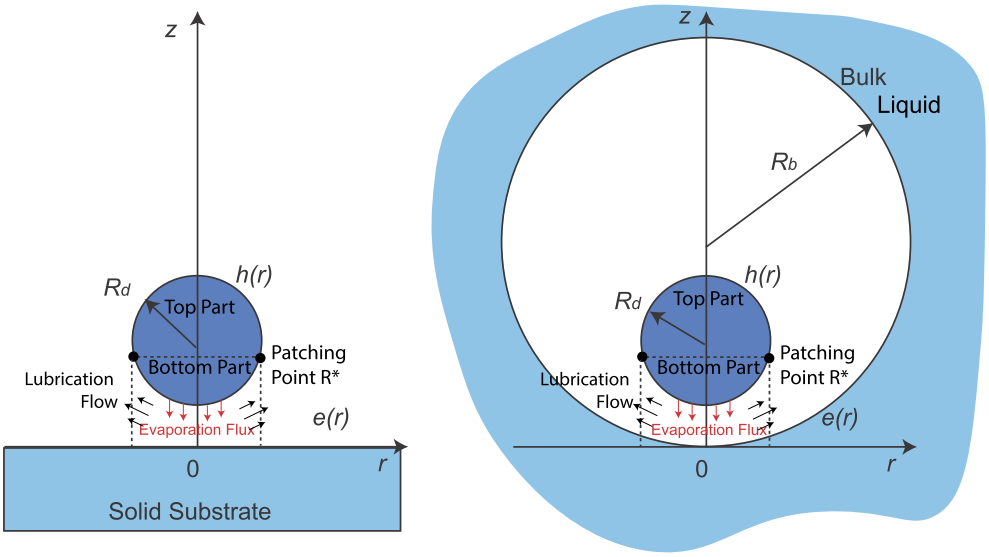

Fig. 1. Geometrical configuration of a liquid nitrogen droplet evaporating above a solid substrate (left) VS inside a hot liquid pool (right). The rapid evaporation of the liquid nitrogen droplet with a radius R_d immersed in hot bulk liquid results in a nitrogen gas bubble surrounding it which has a radius of R_b. The situation in both cases is assumed axisymmetric. A detail of the scene around the vapor layer is shown where the droplet is divided into a top part and a bottom part.

lary length represents the length scale at which capillary forces due to surface tension become comparable to gravitational forces. For a droplet with a radius much less than the capillarity length, the droplet tends to retain a spherical shape since the capillarity force dominates. For saturated liquid nitrogen at atmospheric pressure, the capillary length is approximately 1.1 mm. Neville et al. [16] visualized and quantified the evaporation process of a single liquid nitrogen droplet in immiscible liquids, successfully measuring the evolving droplet and bubble sizes during immersion in a superheated bulk liquid. Bubble growth rates were modeled using a heuristic one-dimensional, pure diffusive, spherically symmetric quasi-steady-state confined model, assuming that the droplet remains in the center of the bubble at all times and the temperature of the bubble and nitrogen droplet is constant. Although the conduction heat transfer rate captures the trend, it consistently underestimates the bubble growth rate due to the oversimplification of the fixed droplet position. The discrepancy was addressed by introducing an empirical effective thermal conductivity, which can significantly limit the applicability of the model due to the uncertainty of this empirical fitting parameter. Meanwhile, Neville et al. [16] observed that the droplet spends most of its life near the lower boundary of the bubble, most likely due to the gravity acting on the droplet and the buoyancy acting on the bubble. This leads to the question that whether the evaporation rate can be well approximated by modeling a quasi-steady drop evaporating in the absence of inertial force such that it stays at the bottom of the bubble.

The objective of this study is to develop a robust quasi-steady theoretical model, devoid of any fitting parameters, to accurately predict the evaporation rate of a droplet while it hovers within a buoyancy-neutral bubble. By determining the precise position of the droplet within the bubble, valuable insights into the evaporation dynamics are gained, such as the vapor layer geometry, and the resultant bubble/droplet size changing rate. Furthermore, scaling laws were found for various parameters, contributing to a comprehensive investigation of the process. The model's predictions are then compared to experimentally measured bubble growth rates from literature [16] and good agreement was obtained confirming the validity of the model.

2. Theoretical model

This section first provides a concise literature review on the study of Leidenfrost droplets, focusing on their evaporation process. Later on, a theoretical model is proposed for investigating the evaporation dynamics of a liquid nitrogen droplet immersed in a water pool and a numerical scheme is discussed at the end of the section.

When a liquid nitrogen droplet is placed on a surface much hotter than the liquid nitrogen boiling point, it levitates on its own vapor which gives the droplet very high mobility and are referred to as the Leidenfrost effect [17]. Accordingly, such floating droplets are referred to as Leidenfrost droplets [18]. The vapor film results in a severe reduction of the heat transfer rate between the droplet and the surface compared with a droplet being in direct contact with the surface. Leidenfrost droplets evaporating above a hot substrate & liquid pool have been widely investigated by researchers through theoretical and experimental methods to determine the heat transfer rate [17,19–22]. In the model proposed by Sobac [20] regarding a Ledeifrost droplet evaporating above a solid substrate, the droplet is split into two regions: the top part and the bottom part as shown on the left in Fig. 1. It is assumed that equilibrium exists for the top part of the droplet where the hydrostatic pressure in the droplet and the Laplace pressure are balanced with each other. Therefore, the top part is not affected by the vapor flow between the droplet and the pool. As for the bottom part of the droplet, the pressure of the vapor flow between the droplet and the bubble is significant and should be taken into account the local force balance. Therefore, the precise shape and position of the droplet were determined by solving the coupled PDEs (Partial Differential Equations).

However, when a liquid nitrogen droplet (≈77 K) is injected into a liquid pool at room temperature (≈294 K), the large temperature difference results in a double-interface configuration: the droplet hovers within a bubble formed by nitrogen vapor. As the droplet evaporates in time the gas bubble grows in size. The rate of growth of the bubble is governed by the heat transfer from the bulk liquid to the droplet. Previous studies of Leidenfrost droplets have not dealt with this scenario. Therefore, a theoretical model is proposed to determine the heat transfer rate between the liquid nitrogen droplet and the liquid pool.

The proposed theoretical model applies the established approaches in modeling a Leidenfrost drop levitated above a flat substrate [20] in the new double-interface configurations. The curvature of a solid substrate is changed into a sphere representing the outer surface of the bubble as illustrated on the right in Fig. 1. The local conductive heat transfer rate at the droplet's outer surface is calculated, and the total heat transfer rate is determined by integrating the local heat transfer

rate over the entire surface of the droplet. The radius change of the liquid nitrogen droplet and the bubble is based on the quasi-state assumption and conservation of energy.

2.1. Assumptions

To simplify the problem, several assumptions are made:

1. It is assumed that the bubble has a spherical shape and the boundary of the bubble has a constant temperature T_b that is equal to the pool liquid temperature T_p. The spherical bubble shape is justified later in Section 3.1.
2. The LN_2 droplet has a uniform temperature T_d that is equal to the saturation temperature [21].
3. The bulk liquid is considered to be incompressible.
4. It is assumed that the bulk liquid and nitrogen gas are immiscible because the solubility of nitrogen gas is in the order of 10^{-5} mole fraction in water in 294 K and atmospheric pressure [23]. Therefore, the mass transfer across the bubble boundary is ignored.
5. Only conductive heat transfer is considered. The convective heat transfer resulting from the flow of the nitrogen gas and the bulk liquid is ignored, which is validated in Section 3.2.
6. It is assumed that a quasi-steady temperature profile is established at each time step [21].

The shape of the droplet and the bubble are considered to be axisymmetric. The shape of the droplet is calculated from the model since the results turned out that the droplet shape is nearly spherical, R_d is used to represent the radius of the droplet in Fig. 1. As shown in Fig. 1, the boundary of the bubble, $e(r)$ is known resulting from the spherical bubble shape assumption. The thickness of the vapor film $h_v(r)$ can be calculated as $h(r) - e(r)$ where $h(r)$ is the boundary of the droplet. The lowest position of the bubble is chosen as $z = 0$.

All properties of the droplet and the pool liquid are evaluated at T_d and T_p, respectively. Since the thermal conductivity of nitrogen gas varies linearly with temperature, the vapor properties are evaluated at the average temperature $\bar{T}_v = (T_d + T_p)/2$. In order to nondimensionalize the problem, all lengths scales are rationalized using the capillary length l_{c_d} of the droplet. All pressure scales are nondimensionalized with σ_d/l_{c_d}. To distinguish between dimensional and dimensionless quantities, all dimensionless quantities are labeled with a tilde (e.g. the dimensionless droplet radius is written as $\tilde{R} = R/l_{c_d}$).

2.2. The position of the droplet

For the liquid nitrogen droplet, the hydrostatic pressure inside the droplet, $\rho_d g z$, locally balances the Laplace pressure jump over the curved droplet interface, $\sigma_d \kappa$, where κ is the curvature of the droplet surface. Using dimensionless quantities, this force equilibrium can be written as

$$\tilde{\kappa}_{top} + \tilde{z}_{top} = \tilde{\kappa}_{outer} + \tilde{z}, \tag{1}$$

where $\tilde{\kappa}_{top}$ is the curvature at the top of the droplet and $\tilde{z}_{top}$ is the z-coordinate of the top of the droplet. The full-form expression for the curvature of an axisymmetric surface is defined as

$$\tilde{\kappa} = \frac{\frac{\partial^2 \tilde{h}}{\partial \tilde{r}^2} + \frac{1}{\tilde{r}}\left(1 + \left(\frac{\partial \tilde{h}}{\partial \tilde{r}}\right)^2\right)\frac{\partial \tilde{h}}{\partial \tilde{r}}}{\left(1 + \left(\frac{\partial \tilde{h}}{\partial \tilde{r}}\right)^2\right)^{3/2}}. \tag{2}$$

The value of $\tilde{\kappa}_{top}$ uniquely determines the shape and size of the droplet. For a certain value of $\tilde{\kappa}_{top}$, this equation can be integrated numerically to find the corresponding equilibrium shape of the droplet. This numerical integration can be done more conveniently in terms of the arclength $\tilde{s}$, in order to deal with the overhang of the sessile droplet [24]. The value of $\tilde{z}_{top}$ does not affect the resulting equilibrium shape, but only the absolute vertical position. The value of $\tilde{z}_{top}$ will be later determined when the two regions are patched together. This equilibrium shape of the top part of the droplet is assumed to be valid above the patching point at $\tilde{r} = \tilde{R}_*$. Below this point, the pressure field in the vapor flow results in a non-equilibrium shape.

As for the bottom part of the droplet, the flow field within the vapor layer needs to be determined to solve for the shape of the droplet. Since the height of the vapor layer is relatively small compared to the diameter of the droplet, the lubrication approximation is used [21,25]. Under the lubrication approximation, the Navier-Stokes equation reduces to

$$\frac{\partial p_v}{\partial z} = 0, \tag{3}$$

$$\frac{\partial p_v}{\partial r} = \mu_v \frac{\partial^2 u}{\partial z^2}, \tag{4}$$

where p_v is the pressure within the vapor layer, and μ_v is the vapor viscosity. Integrating the momentum equation twice with no-slip boundary conditions on both sides results in the following radial velocity profile

$$u_r = \frac{1}{2\mu_v}\frac{\partial p_v}{\partial r}\left(z^2 - zh\right). \tag{5}$$

Integrating this over the height of the vapor layer, gives the following volumetric flux

$$\vec{\mathcal{V}} = -\frac{1}{12\mu_v}\frac{\partial p_v}{\partial r}(h-e)^3. \tag{6}$$

Since the height of the vapor layer is relatively small, it is assumed that heat across the vapor film is transferred only via conduction in the z-direction. Under this assumption, the local heat flux at the bottom droplet boundary, q_{bottom}, is equal to

$$q_{bottom} = \lambda_v \frac{T_p - T_d}{h - e} = \lambda_v \frac{\Delta T}{h - e}, \tag{7}$$

where λ_v is the vapor thermal conductivity, and ΔT is the temperature difference between the droplet and the pool liquid. The local evaporation flux at the droplet boundary is then expressed as

$$\dot{m} = \frac{q_{bottom}}{\Delta h_f} = \frac{\lambda_v}{\Delta h_f}\frac{\Delta T}{h - e}, \tag{8}$$

where Δh_f is the latent heat of evaporation for liquid nitrogen. Finally, the conservation of mass of the evaporated liquid is expressed as

$$\vec{\nabla} \cdot \vec{\mathcal{V}} = \frac{\dot{m}}{\rho_v}, \tag{9}$$

where ρ_v is the vapor density. Substituting Eq. (6) and (8) in Eq. (9) and making every quantity dimensionless, yields

$$-\frac{1}{12}\frac{1}{\tilde{r}}\frac{\partial}{\partial \tilde{r}}\left(\tilde{r}\left(\tilde{h} - \tilde{e}\right)^3 \frac{\partial \tilde{p}_v}{\partial \tilde{r}}\right) - \frac{\tilde{\mathcal{E}}}{\tilde{h} - \tilde{e}} = 0, \tag{10}$$

where $\tilde{\mathcal{E}}$ is the dimensionless evaporation number, which is defined as

$$\tilde{\mathcal{E}} = \frac{\lambda_v \mu_v \Delta T}{\sigma_d \rho_v l_{c_d} \Delta h_f}. \tag{11}$$

Finally, the (gauge) pressure in the vapor layer p_v can be determined by balancing all the forces normal to the droplet surface, leading to

$$\tilde{p}_v = \tilde{\kappa}_{top} + (\tilde{z}_{top} - \tilde{h}) - \tilde{\kappa}. \tag{12}$$

Substituting the expression for $\tilde{p}_v$ in Eq. (10) results in the following final equation, relating the pressure in the vapor layer to the geometry and evaporation of the droplet as

$$-\frac{1}{12}\frac{1}{\tilde{r}}\frac{\partial}{\partial \tilde{r}}\left(\tilde{r}\left(\tilde{h} - \tilde{e}\right)^3 \frac{\partial}{\partial \tilde{r}}\left(\tilde{\kappa}_{top} + (\tilde{z}_{top} - \tilde{h}) - \tilde{\kappa}\right)\right) - \frac{\tilde{\mathcal{E}}}{\tilde{h} - \tilde{e}} = 0. \tag{13}$$

In order to solve this differential equation, several boundary conditions are needed. First of all, since the droplet is axisymmetric, both $\tilde{h}'(\tilde{r})$

and $\tilde{\kappa}'(\tilde{r})$ should be 0 at $\tilde{r}=0$ to fulfill the symmetry conditions. Furthermore, at $\tilde{r}=\tilde{R}_*$, the inner solution must match the upper shape of the droplet. So $\tilde{h}'(\tilde{r})$, $\tilde{\kappa}(\tilde{r})$ and $\tilde{h}(\tilde{r})$ should be equal to the equilibrium upper shape of the droplet at $\tilde{r}=\tilde{R}_*$. Note that the continuity condition for $\tilde{h}(\tilde{r})$ only determines the value of $\tilde{z}_{top}$ and, therefore, does not influence the actual droplet shape of the bottom part. So the boundary conditions are summarized as follows

$$\begin{aligned}&\tilde{h}'(\tilde{R}_*)=\tilde{h}'_{outer}(\tilde{R}_*) \qquad \tilde{h}'(0)=0\\&\tilde{\kappa}(\tilde{R}_*)=\tilde{\kappa}_{outer}(\tilde{R}_*) \qquad \tilde{\kappa}'(0)=0\\&\tilde{h}(\tilde{R}_*)=\tilde{h}_{outer}(\tilde{R}_*)\end{aligned} \tag{14}$$

Note that with these boundary conditions, $\tilde{p}_v$ is continuous at $\tilde{r}=\tilde{R}_*$ by definition, since p_v is defined to be 0 at the top part of the droplet and both $\tilde{h}$ and $\tilde{\kappa}$ are continuous at $\tilde{r}=\tilde{R}_*$.

2.3. Heat transfer

After the relative position is calculated from the above-mentioned method, the conductive heat transfer rate between the droplet and the bubble is determined. The exact solution for calculating the local heat flux in the case of two eccentric spheres maintained at constant temperatures is available using different approaches e.g. the Green theorem method [26], image method [27] and Fourier series expansion [28]. The heat transfer case of two eccentric spheres is normally solved in the bispherical coordinates system. In the present study, the exact solution derived using the Green theorem is used [26].

Bispherical coordinates system is obtained by rotating bipolar axes about the line between the two foci F_1 and F_2. The bispherical system defined by (ξ,θ,ϕ) is illustrated in Fig. 2. The conversion scales between the bispherical coordinates and the cartesian coordinates are

$$x=\frac{a\sin\theta\cos\phi}{\cosh\xi-\cos\theta}, y=\frac{a\sin\theta\sin\phi}{\cosh\xi-\cos\theta}, z=\frac{a\sinh\xi}{\cosh\xi-\cos\theta}. \tag{15}$$

For a point P, θ is the angle of F_2PF_1 and goes from 0 to π. The coordinate ξ is from $-\infty$ to ∞ and is expressed as

$$\xi=\ln\frac{d_1}{d_2} \tag{16}$$

and ϕ is the azimuth angle ranging from 0 to 2π. The scale factors in the bispherical coordinates system are given by

$$h_\theta=h_\xi=\frac{a}{\cosh\xi-\cos\theta}, h_\phi=\frac{a\sin\theta}{\cosh\xi-\cos\theta}, \tag{17}$$

In the bispherical system, the inner sphere ξ_i and outer sphere ξ_o and a are uniquely determined by

$$\xi_i=\sinh^{-1}\frac{a}{r_i}, \xi_o=\sinh^{-1}\frac{a}{r_o} \tag{18}$$

where ϵ is the eccentricity [26].

We further define a dimensionless temperature Θ

$$\Theta=\frac{T-T_i}{T_o-T_i}. \tag{19}$$

The temperatures of the inner sphere (the droplet) and the outer sphere (the bubble) are $T_i=T_d$ and $T_o=T_b$, respectively. The local heat transfer rate from or to any of the two spheres is given as

$$q(\theta)=-\lambda_v\left(\frac{1}{h_\xi}\frac{\partial T}{\partial\xi}\right)_{\xi=\xi^*}=-\lambda_v(T_o-T_i)\left(\frac{1}{h_\xi}\frac{\partial\Theta}{\partial\xi}\right)_{\xi=\xi^*} \tag{20}$$

where ξ^* can be either ξ_o or ξ_i [26].

The total heat transfer rate is the integration of the local heat transfer rate over the surface of the corresponding sphere and is calculated as

$$Q=\int_S q(\theta)\,\mathrm{d}A \tag{21}$$

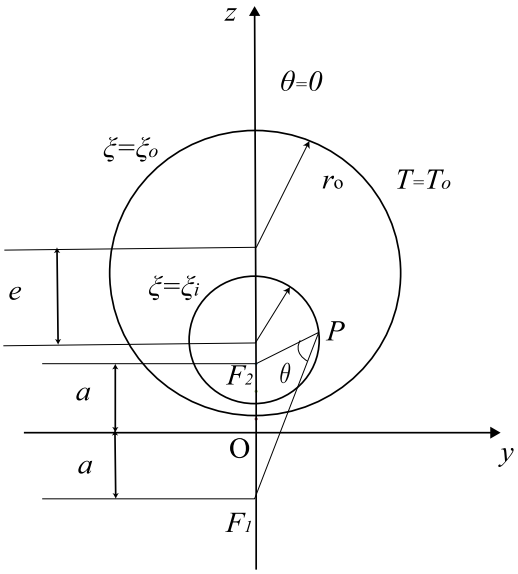

Fig. 2. Illustration of the bispherical coordinates system adapted from [26].

where S is the outer surface of the liquid nitrogen droplet.

2.4. Radius change of the droplet and the bubble

After the total heat transfer rate between the droplet and the bubble is determined, the total evaporation mass flux is calculated. The total evaporation mass flux is written as

$$\frac{\mathrm{d}m}{\mathrm{d}t}=\frac{Q}{\Delta h_f}. \tag{22}$$

Therefore, the radius change of the droplet after a time interval dt yields

$$\mathrm{d}R_d=-\frac{\mathrm{d}m}{4\pi R_d^2\rho_d}, \tag{23}$$

and the radius change of the bubble is also calculated from the conservation of mass

$$\mathrm{d}R_b=\frac{\mathrm{d}m}{4\pi R_b^2\rho_b}. \tag{24}$$

2.5. Numerical scheme

In this section, we introduce the numerical scheme employed in this study to simulate the evaporation of droplets and the growth of bubbles.

For the given initial droplet radius and the initial bubble radius, the position of the droplet is found using the methodology described in section 2.2. Subsequently, the heat transfer rate between the droplet and the bubble is calculated from section 2.3. Since the heat transferred to the droplet contributes to its evaporation, the droplet shrinkage rate is derived. Based on the conservation of mass, the growth of the bubble is determined. Once the radii of the droplet and the bubble for the next step are determined, the simulation for the next quasi-steady state starts. In the simulation implemented in this paper, a convergence study was performed and dt = 0.1 ms was retained.

3. Results and discussion

In this section, the simulation results of the evaporation process of a liquid nitrogen droplet inside a water pool are presented. The droplet shrinkage rate and the bubble growth rate are analyzed. Furthermore, we discuss the evolution of the vapor layer thickness and examine the heat transfer rate between the droplet and the pool.

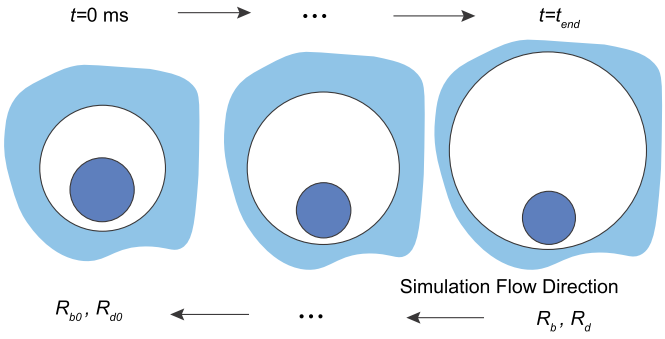

Fig. 3. Illustration of the simulation methodology.

3.1. Droplet shrinkage and bubble growth

The model employed in this study assumes a spherical shape for the bubble, making it crucial to determine the maximum bubble radius within a water pool for maintaining its spherical form. The determination of this maximum radius involves the utilization of two dimensionless numbers: the Galilei number (Ga), which represents the ratio of gravitational force to viscous force ($\equiv \rho_p \sqrt{g R_b} R_b / \mu_p$), and the Eötvös number, which signifies the ratio of gravitational force to surface tension force (Eo ($\equiv \rho_p g R_b^2 / \sigma_p$)) [29]. By plotting Ga and Eo numbers in a phase plot for a given bubble radius, the regime of the shape of the bubble is determined [29]. In the case studied here, with a water pool at room temperature (294 K), the maximum radius for a bubble to maintain a spherical shape is found as $R_{b_{max}} = 0.61$ mm.

The simulation was performed in a reverse time scale, as illustrated in Fig. 3, commencing from the maximum spherical bubble size ($R_{b_{max}}$) and selecting a droplet radius ($R_{d_{end}}$) as the starting point for the calculation at $t = t_{end}$. Subsequently, the simulation progresses backward in time with a fixed time interval until reaching $t = 0$. Below the radius ratio R_b/R_d is around 2 (V_b/V_d around 8), an equilibrium position of the droplet in a bubble cannot be determined which is the criteria for the end of the simulation.

Fig. 4 provides a visualization of the dynamic behavior of a liquid nitrogen droplet during the evaporation process inside a water pool at various time instants. The simulated results demonstrate that the droplet maintains a spherical shape throughout the studied process, thereby confirming the validity of the assumption regarding the droplet's spherical geometry. In Fig. 5, the change of the droplet radius with time is presented. It reveals that $(R_{d_0} - R_d) \sim t$. Similarly, Fig. 6 illustrates the bubble volume as a function of time and reveals that $(V_b - V_{b_0}) \sim t$, which is consistent with the experimental measurements [16].

3.2. Heat flow to the droplet

The local heat flux at the outer boundary of the droplet is illustrated in Fig. 7. The local heat flux reveals a significant contrast between the bottom and top regions of the droplet. Specifically, the heat flux at the bottom interface ($\sim$ 300 kW m^{-2}) is up to six times higher than that at the top interface ($\sim$ 50 kW m^{-2}). This indicates a significant disparity in the heat transfer rates between these two regions. As expected, the bottom interface exhibits a higher heat flux, suggesting a more efficient heat transfer, while the top interface experiences a relatively lower heat flux, indicating a reduced heat transfer rate. The substantial difference in heat flux values at the droplet's outer surface underscores the importance of considering the spatial variation of the droplet within the bubble and emphasizes the dominant role of the bottom region in this heat transfer process.

Since the heat and mass transfer process in liquid droplets is predominantly governed by the bottom region, thus, the vapor layer thickness holds significant importance in understanding the Leidenfrost effect and

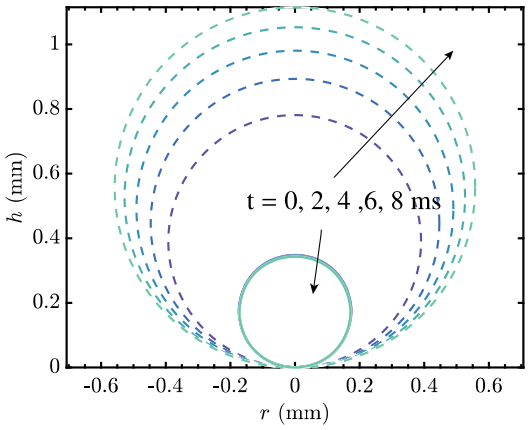

Fig. 4. The growth of the bubble (dashed line) and the shrinkage of the droplet (solid line). The radii of the droplet and the bubble at $t = 0$ are R_{d_0} =174.6 μm and $R_{b_0} = 0.39$ mm, respectively.

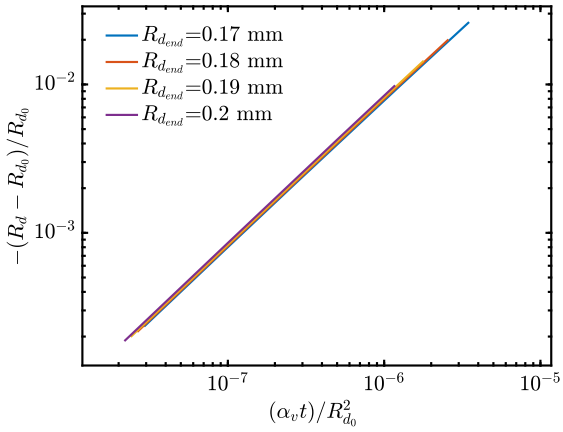

Fig. 5. The dimensionless radius change of the droplet with the dimensionless time scale on a logarithmic scale. The choice of $\alpha t / R_{d_0}^2$, where α_v is the thermal diffusivity of nitrogen vapor, is the dimensionless time based on the open space evaporation time, which is explained in detail in [16]. The change in the droplet radius is normalized by the initial droplet radius. A scaling law $(R_{d_0} - R_d) \sim t$ is found in the plot. The total simulation duration in dimensional form is provided in Table 1. (For interpretation of the colors in the figure(s), the reader is referred to the web version of this article.)

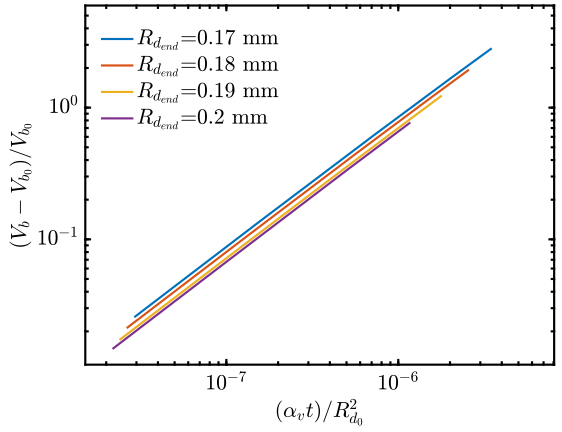

Fig. 6. The dimensionless bubble volume change of the droplet on a logarithmic scale. The change in the droplet radius is normalized by the initial droplet radius. A scaling law $(V_b - V_{b_0}) \sim t$ is found in the plot.

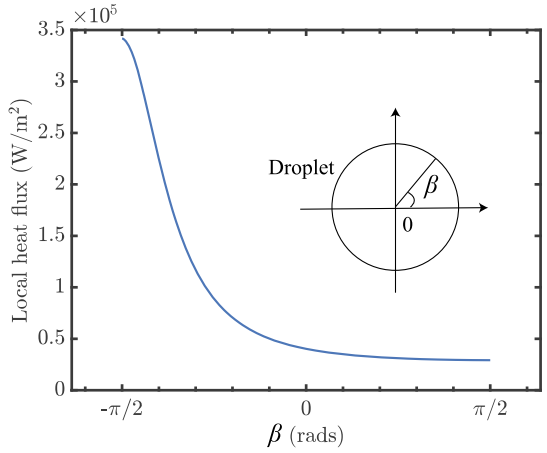

Fig. 7. The local heat flux at the droplet outer boundary as a function of β. The definition of β is shown in the figure and ranges from $-\pi/2$ to $\pi/2$. The heat flux is the largest at the bottom of the droplet ($\beta = -\pi/2$) and decreases as reaching the top ($\beta = \pi/2$).

evaporation dynamics, as it significantly influences the heat transfer rate. Fig. 8 illustrates the observed vapor layer thickness in the study cases alongside the total heat transfer rate. Please note that the vapor layer thickness mentioned here specifically refers to the thinnest distance between the bottom of the droplet and the bubble. The figure demonstrates that the thinnest vapor layer thickness (δ, solid line) corresponds to the highest heat transfer rate (Q_{total}, dashed line) across different droplet sizes. Over time, as the droplet shrinks, δ decreases, promoting conduction heat transfer at the bottom. However, the growing bubble size concurrently increases the thermal resistance, resulting in an overall lower heat transfer rate. It is evident that the vapor layer thickness (on the order of 10 microns) consistently decreases as the droplet size reduces. The decrease of the vapor layer thickness with time is also observed in the solid-substrate Leidenfrost effect [30].

The observed decrease in the vapor layer thickness can be attributed to the interplay between the dynamic change in the weight of the droplet and the pressure within the vapor flow underneath the droplet. As the droplet undergoes evaporation, its weight decreases resulting in a decreased gravitational force. Simultaneously, the shrinkage in the droplet and the growth of the bubble result in a less effective contact area between the droplet and the bubble at the bottom part, leading to a reduced lubrication force. The reduction of lubrication forces within the vapor layer occurs at a faster rate than the gravitational force [31]. Consequently, the droplet experiences a downward acceleration, leading to the observed contraction in the vapor layer thickness. To investigate the scaling relationship in more detail, Fig. 10 utilizes a logarithmic scale to depict δ, although no noticeable scaling law is found between δ and the droplet radius. Furthermore, since the droplet and the bubble both vary in size during the process, the volume ratio is chosen to reveal the scaling law of the heat transfer rate. The total heat transfer rate (Q_{total}) exhibits a scaling behavior of $Q_{total} \sim (V_b/V_d)^{-0.1}$ as shown in Fig. 9.

Since the convective effect is neglected in the model, it is necessary to evaluate the validity of the assumption based on the simulation results. Fig. 7 reveals that the heat transfer is mainly through the thin vapor film trapped between the droplet and the bubble. The thin vapor layer means that the lubrication approximation can be applied which leads to a linear temperature profile locally hence the heat transfer at the bottom part is diffusion dominated. When quantifying the heat transfer for the top part, both the thermal Peclet number for the Stefan flow ($\mathrm{Pe} = R_d u/\alpha$, where u is the droplet shrinkage rate, and α is thermal diffusivity) and the Rayleigh number for the buoyancy flow ($\mathrm{Ra} = g\beta_T \Delta T (R_b - R_d)^3/(\nu\alpha)$, where β_T is the thermal expansion coefficient, ν is the kinetic viscosity) are calculated to be small enough (Pe≈0.027, Ra≈16) such that both convective flows do not contribute significantly to the heat transfer. Ra is calculated to be in the order of 10, indicating a negligible effect of convective heat transfer in the early evaporation stage. In addition, the colder and denser Stefan flow generated from the evaporation of a droplet sitting close to the bottom could serve to further stratify the cold gas at the bottom from the warmer and lighter gas on the top, such that the buoyancy induced convection can be further suppressed.

Table 1
The simulation parameter.

Trial No.	1	2	3	4
$R_{d_{end}}$ (mm)	0.17	0.18	0.19	0.20
t_{end} (ms)	13.3	11.5	10.1	9.6

When the bubble grows further and becomes non-spherical, the flattened bottom and upper surface of the ellipsoidal bubble shape enhance the conduction at the top and bottom of the droplet due to reduced conductive thermal resistance. The buoyancy force acting on the bubble induces oscillations, promoting convective heat transfer within the bubble. The flattened bottom of the bubble also allows for increased rotation of the droplet, enhancing heat and mass transfer. Moreover, the flow field on the top of the droplet may break the assumption of equilibrium for the top part of the droplet. These effects result in a larger heat transfer rate between the droplet and the bubble in the later stages of evaporation (approximately 1.6 times larger than the pure conduction heat transfer rate [16]). A detailed 3D model is necessary to fully model the evaporation process.

3.3. Comparison with experimental data

Experiments were conducted by Neville et al. [16] to observe the evaporation process of a single liquid nitrogen droplet when immersed in various bulk liquids (namely, 2-Propanol, n-Hexane, n-Pentane, and Methanol) [16]. Two identical back-light imaging systems were employed to track the bubble interface and quantify the evaporation process. An in-house code was used to determine the volume of the bubble with a high accuracy of up to 6.68%. During the experiments, the bubble exhibited a near-spherical or ellipsoidal shape, while the droplet remained obscured by the denser nitrogen vapor and could not be distinguished from the images. The buoyancy force caused the bubble to rise inside the bulk liquid.

Experimental data show that, during the initial stages of evaporation, the bubble maintains an almost spherical shape, and heat transfer is primarily dominated by conduction. As time progresses, the bubble evolves into an ellipsoidal shape due to the continuous evaporation of the liquid droplet. At this point, the previously assumed spherical shape is no longer applicable. To provide additional validation for the assumption regarding the spherical shape of smaller bubbles, the experimental data were plotted in a bubble phase diagram, which shows the shape of the bubble in different flow conditions [29], as in Fig. 11. An equivalent radius is used in calculating the Ga and Eo number which is $R_b = \left((3V_b)/(4\pi)\right)^{\frac{1}{3}}$, where V_b is the bubble volume determined from the experiments.

From the bubble shape diagram Fig. 11, it reveals that at low Ga and Eo numbers, gravitational effects are not pronounced and surface tension dominates which results in a spherical bubble shape (Region A). The simulated results presented in this study lie in the spherical bubble regime (i.e. Region A) because the radius of the bubble in all the calculations is smaller or equal to the maximum size for maintaining a spherical shape in water as discussed in Section 3.1. The Eo numbers for experiments in the different bulk liquids almost lie in a similar range since the surface tension of these bulk liquids does not vary significantly. However, it can be seen the Ga number of the experimental data differs significantly resulting from the big difference in the dynamic viscosity of the bulk liquid which is given in Table 2. The solubility of

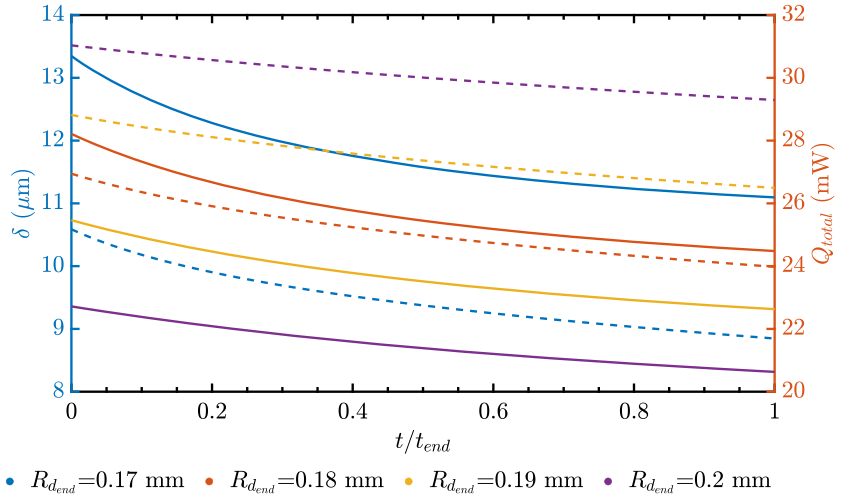

Fig. 8. The vapor layer thickness (δ, solid line) and total heat transfer rate (Q_{total}, dashed line) for different liquid nitrogen droplet sizes, as a function of the dimensionless time. The time is normalized by the total simulation duration.

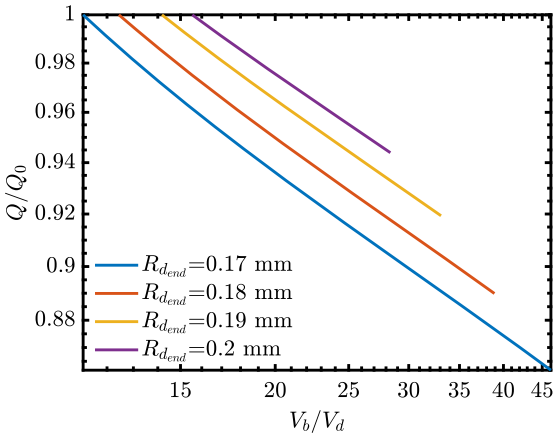

Fig. 9. Normalized heat transfer rate as a function of bubble-droplet volume ratio on a logarithmic scale committing $Q \sim (V_b/V_d)^{-0.1}$. The heat transfer rate is normalized by the respective value at $t = 0$ s.

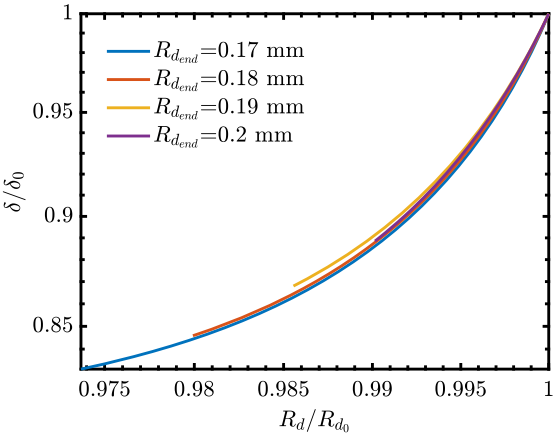

Fig. 10. Normalized vapor layer thickness as a function of their normalized droplet radii on a logarithmic scale. Both the vapor layer thickness and the radius values are normalized based on their respective values at $t = 0$ s.

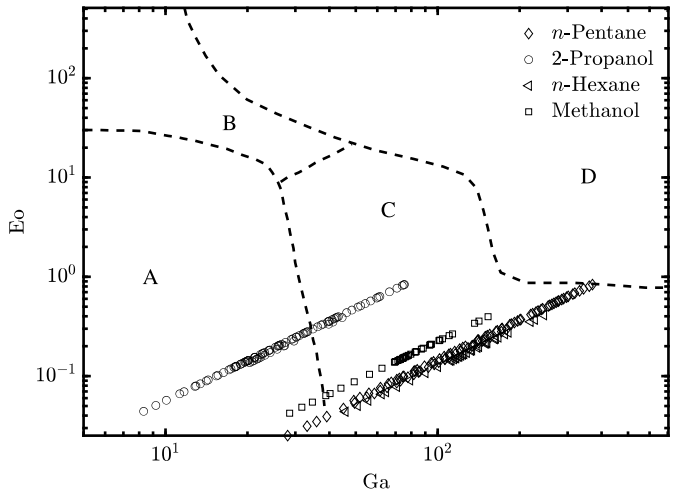

Fig. 11. Bubble phase plot - different regimes of bubble shape and behavior adapted from [29]. Region A refers to the axisymmetric regime, and regions B and C refer to the non-oscillatory and oscillatory asymmetric regime, respectively. Region D represents the breakup regime.

nitrogen gas in these liquids is in the order of 10^{-4} mole fraction indicating the validity of the immiscible assumption [32]. A pool liquid with a smaller dynamic viscosity has a smaller critical radius for retaining a spherical shape which indicates that the model assumption breaks faster compared with the fluid that has a higher viscosity. Since the theoretical model is based on the assumption that the bubble remains spherical, the liquid nitrogen evaporation inside 2-propanol is chosen for the validation of the model.

A comparison of the theoretically predicted results with the experimental data regarding the bubble growth rate is shown in Fig. 12. Fig. 12 (a) illustrates the predicted values from the proposed 2D model and the existing 1D model, together with the experimental data in a non-dimensional plot. The experimental data is observed in good agreement with the experimental data at the early evaporation stage, where the bubble remains spherical. The predicted results from the existing 1D model are slightly lower compared with the proposed 2D model, revealing the same scaling law. Fig. 12 (b) quantitatively compares the bubble volume predicted from different models. It can be observed that at the later stage of evaporation, both models fail to accurately predict the bubble growth rates. This discrepancy may be attributed to the small size of the droplet, where the vapor layer thickness becomes comparable to the droplet radius, leading to deviations from the assumptions of the lubrication theory [33]. Further investigation is necessary to gain a comprehensive understanding of the evaporation process for Lei-

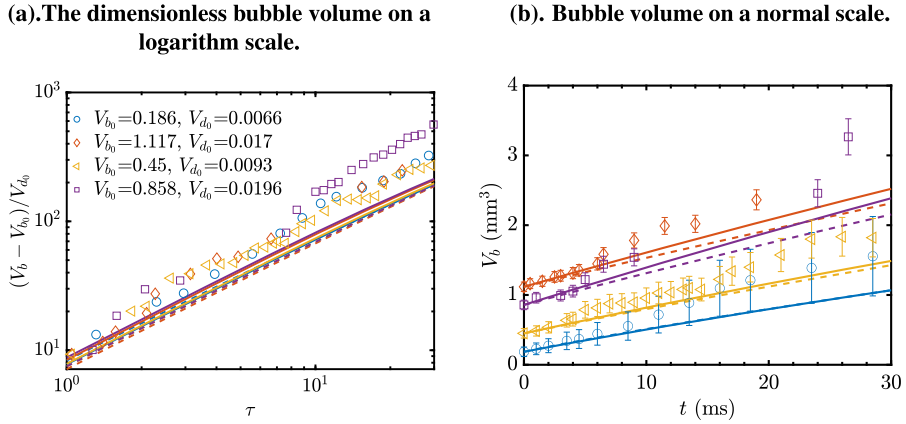

Fig. 12. Comparison of the proposed theoretical predictions (2D model, solid line), the model predicted results from Neville et al. [16] (1D model, dashed line) on bubble volume with the experimental data (scattered points) for liquid nitrogen droplets evaporation inside a 2-propanol pool. V_{d_0}, and V_{b_0} on the legend refer to the initial volume of the droplet and the bubble, respectively. The unit of the bubble and droplet volume shown in the legend is in mm^3. The dimensionless time $\tau = \alpha t/R_{d_0}^2$ is utilized in the x-axis for figure **(a)**. See the online version for references to colors.

Table 2
Thermophysical properties of the bulk liquids at 294 K.

	2-propanol	n-Hexane	n-Pentane	Methanol
Density ρ_p (kg m^3)	780.86	658.58	624.92	790.22
Dynamic viscosity μ_p (Pa s)	1.96×10^{-3}	0.3×10^{-3}	0.22×10^{-3}	0.577×10^{-3}
Surface tension σ_p (m N m^{-1})	21.74	18.50	16	22.95
Thermal diffusivity α_p (m^2 s^{-1})	70.0×10^{-9}	86.6×10^{-9}	78.7×10^{-9}	101.9×10^{-9}

denfrost droplets within this regime where lubrication theory is not applicable. Nonetheless, the proposed theoretical model offers valuable insights into the heat transfer dynamics associated with the evaporation of a liquid nitrogen droplet inside another immiscible liquid pool.

4. Conclusions

A theoretical model with no fitting parameters for accurately predicting the heat transfer rate of a small liquid nitrogen droplet evaporating inside a liquid pool in the spherical bubble regime is proposed. Instead of assuming the droplet is at the center of the bubble, the position of the droplet is found by solving the simplified momentum equation underneath the droplet. It reveals that the position of the droplet in the absence of inertial force is close to the bottom of the bubble which is in agreement with the experimental observation. The majority of the heat and mass transfer between the droplet and the pool happens at the bottom of the droplet resulting from the large temperature gradients across the vapor layer. Although the theoretical model is restricted to the spherical bubble regime because of the spherical bubble shape assumption and limited experimental data can be used to validate the model, a good agreement is found between the theoretical model and the experimental data in terms of the bubble growth rate at the early stage of the liquid nitrogen droplet evaporating inside a 2-propanol pool. However, additional experimental investigations are required to further validate the model. Moreover, it is worth noting from a theoretical perspective that convective heat transfer may become more significant at the later droplet evaporation stage [30].

Nomenclature

α	Thermal diffusivity [m^2 s^{-1}]
β	Angle between the contour of the droplet and the horizontal [rad]
β_T	Thermal expansion coefficient [K^{-1}]
Δh_f	Latent heat of liquid nitrogen [J kg^{-1}]
δ	Vapor layer thickness [m]
$\dot{m}$	Mass flux [kg m^{-2} s^{-1}]
κ	Curvature [m^{-1}]
λ	Thermal conductivity [W m^{-1} K^{-1}]
$\mathcal{E}$	Evaporation number [-]
$\mathcal{V}$	Volumetric flux [m^3 s^{-1}]
μ	Dynamic viscosity [Pa s]
ν	Kinetic viscosity [m^2 s^{-1}]
ρ	Density [kg m^{-3}]
σ	Surface tension [N m^{-1}]
A	Surface area [m^2]
c_p	Specific heat capacity [J kg^{-1} K^{-1}]
e	Height of the bubble surface [m]
g	Gravitational acceleration [m s^{-2}]
h	Height of the droplet surface [m]
l_c	Capillarity length [m]
Q	Heat transfer rate [W]
q	Heat flux [W m^{-2}]
R	Radius [m]
r	Radial coordinate in a cylindrical coordinate system [m]
T	Temperature [K]
t	Time [s]
u	Droplet shrinkage rate [m s^{-1}]
V	Volume [m^3]
z	Vertical coordinate in a cylindrical coordinate system [m]
Eo	Eötvös number
Ga	Galilei number
LN_2	Liquid nitrogen
Pe	Peclet number
Ra	Rayleigh number

Subscripts

0	Initial parameter ($t = 0$)
b	Nitrogen gas bubble

bottom	Bottom part of the liquid nitrogen droplet
d	Liquid nitrogen droplet
end	Parameter at the end ($t = t_{end}$)
outer	Outer part of the liquid nitrogen droplet
p	Pool Liquid
top	Top part of the liquid nitrogen droplet
v	Vapor

CRediT authorship contribution statement

Z. Zhang: Writing – review & editing, Writing – original draft, Methodology, Investigation, Formal analysis, Data curation, Conceptualization. **H. Zhao:** Writing – review & editing, Visualization, Methodology. **S. Vanapalli:** Writing – review & editing, Supervision, Project administration, Funding acquisition, Conceptualization.

Declaration of competing interest

The authors declare that they have no known competing financial interests or personal relationships that could have appeared to influence the work reported in this paper.

Data availability

No data was used for the research described in the article.

Acknowledgements

This work is sponsored by Holland High Tech (TKI-HTSM) via the Dutch Ministry of Economic Affairs and Climate Policy's PPS bonus scheme for Research and Innovation and Air Liquide for the project 'Cooling Characteristic of Cryogenic Leidenfrost Drops and Solids', grant number SBD 2019-114. The authors would like to acknowledge Marijn Kalter for his valuable suggestions and fruitful discussions. The authors would also like to acknowledge Abhishek Purandre, Rick Spikjers, and Arvi Xhaxi for the discussions.

References

[1] D. Ali, J.M. Farber, J. Kim, N. Parto, R. Copes, A qualitative risk assessment of liquid nitrogen in foods and beverages, Food Prot. Trends 41 (3) (2021) 293–304.
[2] J. Miller, The use of liquid nitrogen in food freezing, Food Freez. Today Tomorrow (1991) 157–170.
[3] M. Aref, The present status of liquid nitrogen freezing of foods, Can. Inst. Food Technol. J. 1 (1) (1968) 11–16.
[4] W. Beaver, Liquid nitrogen for concrete cooling, Concr. Int. 26 (9) (2004) 93–95.
[5] I.K. Harith, M.S. Hassan, S.S. Hasan, Liquid nitrogen effect on the fresh concrete properties in hot weathering concrete, Innov. Infrastructure Solutions 7 (1) (2022) 127.
[6] M.C. Juenger, J. Hema, S. Solt, Effects of liquid nitrogen on concrete properties, Tech. rep., Center for Transportation Research, University of Texas at Austin, 2007.
[7] F. Christodoulou, V. Sechenyh, H. Zhao, C.P. Garner, H. Clarke, Performance of a novel liquid nitrogen power system, Appl. Therm. Eng. 191 (2021) 116896.
[8] A. Tafone, F. Dal Magro, A. Romagnoli, Integrating an oxygen enriched waste to energy plant with cryogenic engines and air separation unit: technical, economic and environmental analysis, Appl. Energy 231 (2018) 423–432.
[9] V. Sechenyh, F. Christodoulou, H. Zhao, C. Garner, D. Fennell, The effect of heat exchange fluid composition on the performance of a liquid nitrogen engine system, Energies 14 (5) (2021) 1474.
[10] S. Awonorin, Evaporation rates of freely falling liquid nitrogen droplets in air, Heat Transf. Eng. 10 (1) (1989) 26–36.
[11] D. Wen, H. Chen, Y. Ding, P. Dearman, Liquid nitrogen injection into water: pressure build-up and heat transfer, Cryogenics 46 (10) (2006) 740–748.
[12] H. Clarke, A. Martinez-Herasme, R. Crookes, D. Wen, Experimental study of jet structure and pressurisation upon liquid nitrogen injection into water, Int. J. Multiph. Flow 36 (11–12) (2010) 940–949.
[13] V. Nakoryakov, I. Mezentsev, A. Meleshkin, D. Elistratov, Visualization of physical processes occurring on liquid nitrogen injection into water, J. Eng. Phys. Thermophys. 24 (2015) 322–329.
[14] Z. Lan, D. Zhu, W. Tian, G. Su, S. Qiu, Experimental study on spray characteristics of pressure-swirl nozzles in pressurizer, Ann. Nucl. Energy 63 (2014) 215–227.
[15] X. Liu, R. Xue, Y. Ruan, L. Chen, X. Zhang, Y. Hou, Effects of injection pressure difference on droplet size distribution and spray cone angle in spray cooling of liquid nitrogen, Cryogenics 83 (2017) 57–63.
[16] N. Rebelo, H. Zhao, F. Nadal, C. Garner, A. Williams, Evaporation of liquid nitrogen droplets in superheated immiscible liquids, Int. J. Heat Mass Transf. 143 (2019) 118575.
[17] B.S. Gottfried, K.J. Bell, Film boiling of spheroidal droplets. leidenfrost phenomenon, Ind. Eng. Chem. Fundam. 5 (4) (1966) 561–568.
[18] J.G. Leidenfrost, De Aquae Communis Nonnullis Qualitatibus Tractatus, Ovenius, 1756.
[19] J. Burton, A. Sharpe, R. Van Der Veen, A. Franco, S. Nagel, Geometry of the vapor layer under a leidenfrost drop, Phys. Rev. Lett. 109 (7) (2012) 074301.
[20] B. Sobac, A. Rednikov, S. Dorbolo, P. Colinet, Leidenfrost effect: accurate drop shape modeling and refined scaling laws, Phys. Rev. E 90 (5) (2014) 053011.
[21] L. Maquet, B. Sobac, B. Darbois-Texier, A. Duchesne, M. Brandenbourger, A. Rednikov, P. Colinet, S. Dorbolo, Leidenfrost drops on a heated liquid pool, Phys. Rev. Fluids 1 (5) (2016) 053902.
[22] M.A. Van Limbeek, B. Sobac, A. Rednikov, P. Colinet, J.H. Snoeijer, Asymptotic theory for a leidenfrost drop on a liquid pool, J. Fluid Mech. 863 (2019) 1157–1189.
[23] E. Wilhelm, A. van Hook, U. Domanska-Zelazna, R.P. Tomkins, D. Richon, V. de Stafani, C. Coquelet, M.C. Gomes, J.I. Siepmann, K.E. Anderson, et al., Developments and Applications in Solubility, Royal Society of Chemistry, 2007.
[24] J.H. Snoeijer, P. Brunet, J. Eggers, Maximum size of drops levitated by an air cushion, Phys. Rev. E 79 (3) (2009) 036307.
[25] Z. Zhang, R. Spijkers, M. Schremb, S. Vanapalli, Heat and mass transfer during levitation of a liquid nitrogen leidenfrost droplet on a water pool, in: IOP Conference Series: Materials Science and Engineering, vol. 1240, IOP Publishing, 2022, p. 012157.
[26] A. Yılmazer, C. Kocar, Exact solution of the heat conduction equation in eccentric spherical annuli, Int. J. Therm. Sci. 68 (2013) 158–172.
[27] J.-T. Chen, H.-C. Shieh, Y.-T. Lee, J.-W. Lee, Image solutions for boundary value problems without sources, Appl. Math. Comput. 216 (5) (2010) 1453–1468.
[28] R. Alassar, Conduction in eccentric spherical annuli, Int. J. Heat Mass Transf. 54 (15–16) (2011) 3796–3800.
[29] M.K. Tripathi, K.C. Sahu, R. Govindarajan, Dynamics of an initially spherical bubble rising in quiescent liquid, Nat. Commun. 6 (1) (2015) 6268.
[30] S. Chandra, D. Aziz, Leidenfrost evaporation of liquid nitrogen droplets, Prev. Heat Mass Transf. 2 (21) (1995) 128.
[31] J. Park, D.E. Kim, Dynamic leidenfrost behaviors of different fluid drops on superheated surface: scaling for vapor film thickness, Phys. Fluids 31 (10) (2019).
[32] R. Battino, T.R. Rettich, T. Tominaga, The solubility of nitrogen and air in liquids, J. Phys. Chem. Ref. Data 13 (2) (1984) 563–600.
[33] S. Lyu, V. Mathai, Y. Wang, B. Sobac, P. Colinet, D. Lohse, C. Sun, Final fate of a leidenfrost droplet: explosion or takeoff, Sci. Adv. 5 (5) (2019), eaav8081.